

First glycine isomer detected in the interstellar medium: glycolamide (NH₂C(O)CH₂OH)

VÍCTOR M. RIVILLA,¹ MIGUEL SANZ-NOVO,^{1,2,3} IZASKUN JIMÉNEZ-SERRA,¹ JESÚS MARTÍN-PINTADO,¹ LAURA COLZI,¹ SHAOSHAN ZENG,⁴ ANDRÉS MEGÍAS,¹ ÁLVARO LÓPEZ-GALLIFA,¹ ANTONIO MARTÍNEZ-HENARES,¹ SARAH MASSALKHI,¹ BELÉN TERCERO,⁵ PABLO DE VICENTE,⁶ SERGIO MARTÍN,^{7,8} DAVID SAN ANDRÉS,¹ MIGUEL A. REQUENA-TORRES,^{9,10} AND JOSÉ LUIS ALONSO²

¹Centro de Astrobiología (CAB), INTA-CSIC, Carretera de Ajalvir km 4, Torrejón de Ardoz, 28850 Madrid, Spain

²Grupo de Espectroscopia Molecular (GEM), Edificio Quifima, Laboratorios de Espectroscopia y Bioespectroscopia, Parque Científico UVa, Universidad de Valladolid, 47011 Valladolid, Spain

³Computational Chemistry Group, Departamento de Química Física y Química Inorgánica, Universidad de Valladolid, E-47011 Valladolid, Spain

⁴Star and Planet Formation Laboratory, Cluster for Pioneering Research, RIKEN, 2-1 Hirosawa, Wako, Saitama, 351-0198, Japan

⁵Observatorio Astronómico Nacional (OAN-IGN), Calle Alfonso XII, 3, 28014 Madrid, Spain

⁶Observatorio de Yebes (OY-IGN), Cerro de la Palera SN, Yebes, Guadalajara, Spain

⁷European Southern Observatory, Alonso de Córdova 3107, Vitacura 763 0355, Santiago, Chile

⁸Joint ALMA Observatory, Alonso de Córdova 3107, Vitacura 763 0355, Santiago, Chile

⁹University of Maryland, College Park, ND 20742-2421 (USA)

¹⁰Department of Physics, Astronomy and Geosciences, Towson University, Towson, MD 21252, USA

ABSTRACT

We report the first detection in the interstellar medium of a C₂H₅O₂N isomer: *syn*-glycolamide (NH₂C(O)CH₂OH). The exquisite sensitivity at sub-mK levels of an ultra-deep spectral survey carried out with the Yebes 40m and IRAM 30m telescopes towards the G+0.693-0.027 molecular cloud have allowed us to unambiguously identify multiple transitions of this species. We derived a column density of $(7.4 \pm 0.7) \times 10^{12} \text{ cm}^{-2}$, which implies a molecular abundance with respect to H₂ of 5.5×10^{-11} . The other C₂H₅O₂N isomers, including the higher-energy *anti* conformer of glycolamide, and two conformers of glycine, were not detected. The upper limit derived for the abundance of glycine indicates that this amino acid is surely less abundant than its isomer glycolamide in the ISM. The abundances of the C₂H₅O₂N isomers cannot be explained in terms of thermodynamic equilibrium, and thus chemical kinetics need to be invoked. While the low abundance of glycine might not be surprising, based on the relative low abundances of acids in the ISM compared to other compounds (e.g. alcohols, aldehydes or amines), several chemical pathways can favour the formation of its isomer glycolamide. It can be formed through radical-radical reactions on the surface of dust grains. The abundances of these radicals can be significantly boosted in an environment affected by a strong ultraviolet field induced by cosmic rays, such as that expected in G+0.693-0.027. Therefore, as shown by several recent molecular detections towards this molecular cloud, it stands out as the best target to discover new species with carbon, oxygen and nitrogen with increasing chemical complexity.

Keywords: Interstellar molecules(849), Interstellar clouds(834), Galactic center(565), Spectral line identification(2073), Astrochemistry(75)

1. INTRODUCTION

Glycine (or 2-aminoacetic acid, NH₂CH₂COOH) is the simplest representative of amino acids, the building blocks of proteins, which play fundamental catalytic and metabolic roles in biochemistry. Given that some fundamental molecular precursors that contributed to the origin of life on Earth could have an extraterrestrial origin (e.g. Pearce et al. 2017), numerous efforts have been focused on the search for glycine in space in the

last decades. Along with other amino acids, glycine has been detected in chondritic meteorites (Cronin & Pizzarello 1983; Burton et al. 2012), and very recently in samples provided by the JAXA Hayabusa2 mission of the asteroid Ryugu (Potiszil et al. 2023). It was also detected in the comet 67P/Churyumov-Gerasimenko by the *in-situ* mass spectrometric analysis performed by the ESA spacecraft Rosetta (Altwegg et al. 2016). These detections put forward the possibility of glycine to be

originally formed in the interstellar medium (hereafter ISM) and then incorporated to the protosolar nebula (Pizzarello et al. 2006). In the context of this latter hypothesis, glycine, along more complex amino acids and other prebiotic chemicals, might have been delivered to early Earth through cometary and meteoritic impacts (Oró 1961; Cronin et al. 1988; Chyba 1990; Chyba & Sagan 1992; Cooper et al. 2001; Pasek 2008; Glavin & Dworkin 2009; Pearce et al. 2017; Marty et al. 2017; O’Brien et al. 2018; Rubin et al. 2019; Rivilla et al. 2020a).

Laboratory experiments have shown that glycine can be synthesized under interstellar conditions (e.g. Muñoz Caro et al. 2002; Ioppolo et al. 2021). Kuan et al. (2003) claimed the presence of glycine towards several high-mass star-forming regions, although a rigorous verification performed by Snyder et al. (2005) finally disproved these detections. Glycine has not been detected yet in the ISM, despite the multiple observational efforts targeting different astronomical environments (e.g. Combes et al. 1996; Ceccarelli et al. 2000; Snyder et al. 2005; Jones et al. 2007; Cunningham et al. 2007; Jiménez-Serra et al. 2016, 2020).

The non detection of glycine might imply that it is not the most abundant member of the $C_2H_5O_2N$ isomeric family in the ISM. Indeed, glycine is not the most thermodynamically stable isomer, but two other isomers (Sanz-Novo et al. 2019): N-methylcarbamic acid ($CH_3NHCOOH$), whose microwave spectroscopy is not available, and *syn*-methyl carbamate ($CH_3OC(O)NH_2$), whose search has been unfruitful so far (Demyk et al. 2004). Other isomers less stable than glycine, such as glycolamide ($NH_2C(O)CH_2OH$; Sanz-Novo et al. 2020; Colzi et al. 2021), and N-(Z)-hydroxyacetamide ($CH_3C(O)NHOH$; Sanz-Novo et al. 2022a) remain elusive.

In this work, we have searched for all the $C_2H_5O_2N$ isomers for which microwave rotational spectroscopy is currently available, towards the chemically rich G+0.693-0.027 molecular cloud (G+0.693 hereafter), located in the Sgr B2 region of the Galactic Center. Many prebiotically relevant molecules have been detected for the first time in the ISM towards this source in the last four years, which makes it a very promising candidate for new discoveries (Rivilla et al. 2019, 2020b, 2021a,b, 2022a,b; Rodríguez-Almeida et al. 2021a,b; Zeng et al. 2021; Jiménez-Serra et al. 2022). As a result of our search, we report the first detection in the ISM of a member of the $C_2H_5O_2N$ isomeric family: the *syn* conformer of glycolamide ($NH_2C(O)CH_2OH$), as well as very constraining upper limits of the abundances for the other isomers, including two conformers of glycine.

2. OBSERVATIONS

We have significantly improved the sensitivity of the spectral survey towards G+0.693 used in previous works (e.g. Zeng et al. 2020; Rivilla et al. 2021a,b, 2022a,b,c; Rodríguez-Almeida et al. 2021a,b; Zeng et al. 2021; Colzi et al. 2022; Jiménez-Serra et al. 2022; Zeng et al. 2023), performing new ultra-deep observations with the Yebes 40m (Guadalajara, Spain) and IRAM 30m (Granada, Spain) telescopes. The observations, using position switching mode, were centered at $\alpha(\text{ICRS}) = 17^h 47^m 22^s$, $\delta(\text{ICRS}) = -28^\circ 21' 27''$, with the off position shifted by $\Delta\alpha = -885''$ and $\Delta\delta = 290''$. The line intensity of the spectra was measured in units of antenna temperature (T_A^*) since the molecular emission towards G+0.693 is extended beyond the telescope primary beams (Requena-Torres et al. 2006, 2008; Zeng et al. 2018, 2020).

The Yebes 40m observations (project 21A014; PI Rivilla) were carried out during multiple sessions between March 2021 and March 2022, with a total telescope scheduled time of 230 hours, of which 110 hours were on source. Part of this project, based on half of the observing runs, was presented in Rivilla et al. (2022a,b). The Nanocosmos Q-band (7 mm) HEMT receiver was used, which provides ultra broad-band observations (18.5 GHz) in two linear polarizations (Tercero et al. 2021). The receiver was connected to 16 FFTS providing a channel width of 38 kHz. We observed two different spectral setups centered at 41.4 and 42.3 GHz, with a total frequency coverage of 31.07–50.42 GHz. Telescope pointing and focus were checked every one or two hours through pseudo-continuum observations. The half power beam width (HPBW) of the telescope was $\sim 35''$ – $55''$ in the observed frequency range. We performed an initial data inspection and reduction using a Python-based script¹ that uses the CLASS module of the GILDAS package (Megías et al. 2023). For each observing day, we automatically fitted baselines using an iterative method that first masks the more visible lines using sigma-clips, and then applies rolling medians and averages, interpolating the masked regions with splines. Spectra were then combined, averaged, and imported to MADCUBA (Martín et al. 2019). The comparison of the spectra of the two frequency setups was used to identify possible spurious signals and other technical artifacts. The final spectra were smoothed to 256 kHz, which translates into velocity resolutions of 1.5–2.5 km s⁻¹ in the range observed, which are enough to properly characterize the typical linewidths of 15–20 km

¹ <https://github.com/andresmegias/gildas-class-python/>

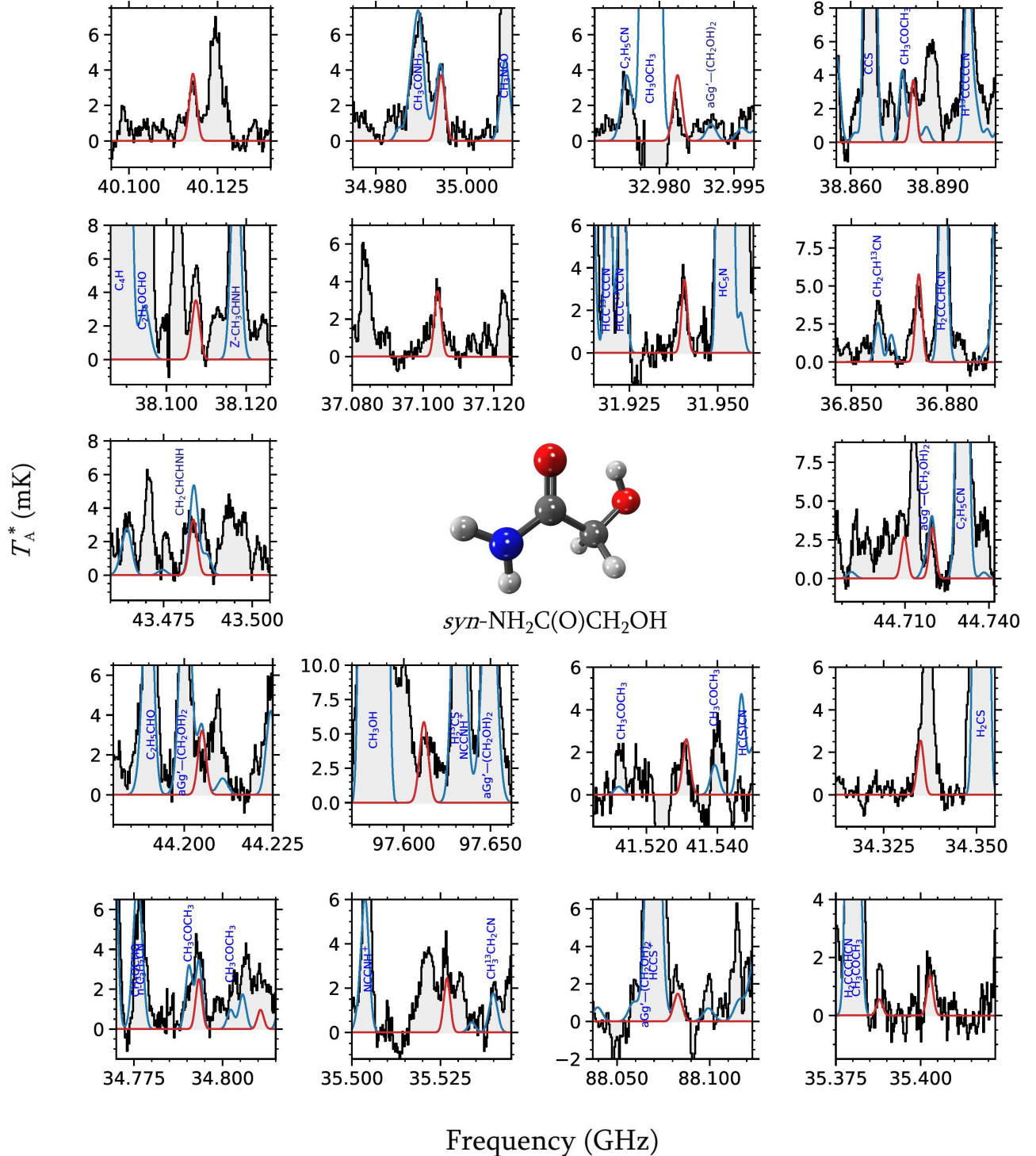


Figure 1. Unblended or slightly blended transitions of glycolamide detected towards the G+0.693, displayed in order of decreasing line intensity. The observed spectra are shown as a grey histogram. The best LTE fit derived with MADCUBA for the *syn*-glycolamide emission is shown with a red curve. The blue curve represents the total modelled emission considering all the species identified towards this molecular cloud. In the center, the molecular structure of the *syn* conformer of glycolamide is shown. Carbon atoms in grey, oxygen atoms in red, nitrogen atom in blue, and hydrogen atoms in white.

s^{-1} observed in the region (e.g. Requena-Torres et al. 2006; Zeng et al. 2018; Rivilla et al. 2022c). We have checked flux density consistency between the new observations and the previous Yebes survey (e.g. Zeng et al. 2020; Rodríguez-Almeida et al. 2021a). We find that the line intensities are consistent within a 5% level. The achieved noise at this spectral resolution is 0.25–0.9 mK, depending on the spectral range.

The IRAM 30m observations (project 123-22, PI Jiménez-Serra) were carried out in the period of February 1–18 2023. We used several frequency setups to cover different spectral ranges of the E0 (3 mm) and E1 (2 mm) bands of the Eight Mixer Receiver (EMIR) receiver. We used the Fast Fourier Transform Spectrometer (FTS), which provides a spectral resolution of 195 kHz. We slightly shifted in frequency each setup to identify possible contamination of lines from the image band. The new spectral ranges covered were 83.2–115.41 GHz, 132.28–140.39 GHz, and 142–173.81 GHz. The HPBW is $\sim 14''$ – $29''$. The spectra were exported from CLASS to MADCUBA, and the reduction, including baseline subtraction, was carried out in MADCUBA. We checked the line intensities of the new observations with those of previous data (e.g. Rodríguez-Almeida et al. 2021a; Rivilla et al. 2021a), which are consistent within a 5% level. We then averaged the new data with those from the previous survey, weighting them by the noise of the spectra. The final spectra were smoothed to 615 kHz (1.0–2.2 km s^{-1} in the spectral range covered). The final noise achieved is 0.5–2.5 mK at 3 mm, and 1.0–1.6 mK at 2 mm. For the spectral ranges not covered by these new observations, we used the data from our previous IRAM 30m survey (for details we refer to Rodríguez-Almeida et al. 2021a; Rivilla et al. 2022b,c).

3. ANALYSIS AND RESULTS

We list in Table 1 the $C_2H_5O_2N$ isomeric family. We have searched for all the isomers for which rotational spectroscopy is available: *syn*-methyl carbamate ($CH_3OC(O)NH_2$), conformers I and II of glycine² (NH_2CH_2COOH), conformers *syn* and *anti* of glycolamide ($NH_2C(O)CH_2OH$), and the *Z*-conformer of *N*-hydroxyacetamide ($CH_3C(O)NHOH$).

The exquisite sensitivity of the new observations presented here has allowed to detect *syn*-glycolamide, which is the first $C_2H_5O_2N$ isomer reported in the ISM. Glycolamide (or 2-hydroxyacetamide) has two conform-

ers having C_s symmetry, with the hydroxyl ($-OH$) *syn* or *anti* with respect to the carbonyl group ($-C=O$). The *syn* conformer is lower in energy by ~ 0.9 kcal mol^{-1} (501 K; Table 1), thanks to the formation of a stabilizing intramolecular hydrogen bond that also hinders a possible large amplitude motion of the $-OH$ moiety.

For *syn*-glycolamide we have implemented the rotational spectroscopy from the laboratory work by Sanz-Novo et al. (2020) into the SLIM (Spectral Line Identification and Modeling) tool within MADCUBA (version 9.3.10, 04/05/2023). To search for the species, we generated with SLIM a synthetic spectrum under the assumption of Local Thermodynamic Equilibrium (LTE) conditions. Figure 1 shows transitions of *syn*-glycolamide detected towards G+0.693 that are unblended or only slightly blended with transitions from other species. Spectroscopic information of these transitions is presented in Table 2. To ensure that the observed spectral features are due to *syn*-glycolamide, and to properly evaluate possible line contamination by other molecules, we have considered the emission from the > 130 molecules already identified towards G+0.693 (e.g. Requena-Torres et al. 2006, 2008; Zeng et al. 2018; Rivilla et al. 2018, 2019, 2020b, 2021a,b, 2022a,b,c; Jiménez-Serra et al. 2020; Jiménez-Serra et al. 2022; Biz-zocchi et al. 2020; Rodríguez-Almeida et al. 2021a,b; Zeng et al. 2021; Colzi et al. 2022; Alberton et al. 2023; San Andrés et al. 2023; Zeng et al. 2023). We note that the rest of the *syn*-glycolamide transitions that fall within the spectral coverage of the survey are consistent with the observed spectra, but they are heavily blended with lines from other molecular species or too faint to be detected.

To derive the physical parameters of the emission, we used the SLIM-AUTOFIT tool of MADCUBA that provides the best non-linear least-squares LTE fit to the data using the Levenberg-Marquardt algorithm. The parameters used in the LTE model are: molecular column density (N), excitation temperature (T_{ex}), velocity (v_{LSR}) and full width at half maximum (FWHM) of the Gaussian line profiles. Since the molecular emission towards G+0.693 is extended and fills the telescope beams (Requena-Torres et al. 2006, 2008; Zeng et al. 2018, 2020), no beam filling factor is used in our calculations. The fit of the *syn*-glycolamide emission was performed by using the transitions shown in Figure 1, and considering also the contribution of the other identified molecules. To allow the convergence of AUTOFIT, we fixed the value of T_{ex} to 5 K, which was derived for the optically thin ^{13}C isotopologue of the simplest amide, formamide, by Zeng et al. (2023). We also fixed the FWHM to 18 km s^{-1} , which reproduces well the

² We note that there are up to thirteen conformers of glycine (Csaszar 1992), but we include in Table 1 only those two with lowest-energy, which are the only ones with rotational spectroscopy well characterized in the laboratory.

Table 1. C₂H₅O₂N isomeric family. Relative energies, availability of microwave spectroscopy, dipole moments, and molecular abundances derived towards G+0.693 are indicated. The “Microwave spectroscopy” column indicates the catalog entry when available, or refers to MADCUBA for catalog entries generated from published spectroscopy.

Name	Formula	ΔE kcal mol ⁻¹ (K)	Microwave spectroscopy	μ Debye	G+0.693 abundance ($\times 10^{-10}$)
N-methylcarbamic acid	CH ₃ NHCOOH	0.0 (0.0) ^a	–	2.5 ^a	–
<i>syn</i> -methyl carbamate	CH ₃ OC(O)NH ₂	4.6 (2335) ^a	JPL 75004 ^e	2.3 ^a	< 2.5
glycine (conformer I)	NH ₂ CH ₂ COOH	8.4 (4247) ^a	CDMS 75511 ^f	1.1 ⁱ	< 0.6
glycine (conformer II)	NH ₂ CH ₂ COOH	9.2 (4650) ^b	CDMS 75512 ^f	5.5 ⁱ	< 0.019
<i>syn</i> -glycolamide	NH ₂ C(O)CH ₂ OH	9.7 (4866) ^a	MADCUBA ^g	4.4 ^a	0.55
<i>anti</i> -glycolamide	NH ₂ C(O)CH ₂ OH	10.6 (5367) ^c	MADCUBA ^g	2.6 ^g	< 0.13
N-(hydroxymethyl)formamide	HOCH ₂ NHCHO	16.7 (8404) ^d	–	3.1 ^d	–
aminomethyl formate	NH ₂ CH ₂ OCHO	17.7 (8907) ^d	–	1.7 ^d	–
aminohydroxyacetaldehyde	NH ₂ CH(OH)CHO	27.6 (13889) ^d	–	1.6 ^d	–
2-aminoethene-1,1-diol	NH ₂ CHC(OH) ₂	30.7 (15449) ^d	–	1.3 ^d	–
O-acetylhydroxylamine	CH ₃ COONH ₂	43.5 (21875) ^a	–	1.9 ^a	–
N-(Z)-hydroxyacetamide	CH ₃ C(O)NHOH	44.7 (22474) ^a	MADCUBA ^h	3.3 ^{a,h}	< 1.7
N-hydroxyacetamidic acid	CH ₃ C(OH)NOH	45.5 (22872) ^a	–	2.5 ^a	–

(a) Calculated at the CCSD(T)/aug-cc-pVTZ//MP2/aug-cc-pVTZ level by Sanz-Novo et al. (2019); (b) Estimated using the B3LYP/6-311G(d,p) energy difference computed by Lattelais et al. (2011); (c) Estimated using the energy difference between *syn*- and *anti*-glycolamide calculated in Maris (2004) from relative intensity and dipole moment measurements; (d) Calculated at the CCSD(T)/cc-pVQZ//B3LYP/cc-pVQZ level by Lattelais et al. (2011); (e) Groner et al. (2007), Ilyushin et al. (2006), Marstokk & Mollendal (1999) and Bakri et al. (2002); (f) Lovas et al. (1995) and Ilyushin et al. (2005); (g) Sanz-Novo et al. (2020) and Maris (2004); (h) Sanz-Novo et al. (2022a); (i) Lovas et al. (1995).

profile of the most unblendend lines, and we left free N and v_{LSR} . The best LTE fit is shown in Figure 1. We obtained a velocity of $v_{\text{LSR}} = 67.0 \pm 1.0$ km s⁻¹, which is in good agreement with the values found in G+0.693 for other molecular species, and in particular amides (Zeng et al. 2023). The derived column density is $(7.4 \pm 0.7) \times 10^{12}$ cm⁻², which translates into a molecular abundance with respect to molecular hydrogen of 5.5×10^{-11} (Table 1), assuming $N_{\text{H}_2} = 1.35 \times 10^{23}$ cm⁻² (Martín et al. 2008).

We also searched for the other C₂H₅O₂N isomers for which spectroscopy is available (see Table 1): the higher-energy *anti*-conformer of glycolamide, the conformers I and II of glycine (NH₂CH₂COOH), *syn*-methyl carbamate (CH₃OC(O)NH₂), and the *Z* isomer of N-hydroxyacetamide (CH₃C(O)NHOH). None of them is detected, so we computed the upper limits of their column densities using the catalog entries and spectroscopic works presented in Table 1. The detailed description of the calculations and the specific transitions used are presented in Appendix A, and the resulting upper limits are listed in Table 1.

4. DISCUSSION

4.1. The first C₂H₅O₂N isomer detected in the ISM

In spite of the many observational efforts done in the past, mainly targeting glycine, no C₂H₅O₂N isomer was

reported in the ISM before the detection of glycolamide presented in this work. We discuss in this section why glycolamide is easier to detect than other isomers, and, in particular, the long-sought glycine.

The detectability of a molecular species through rotational spectroscopy depends, obviously, on the molecular abundance, but also on the strength of the dipole moment (μ). The larger the dipole moment the brighter the line intensities, and thus the easier to detect the molecule. We summarize in Table 1 the dipole moments of the different C₂H₅O₂N isomers, computed from the experimental and theoretical works cited there. The highest dipole moments are those of the higher-energy conformer of glycine (conformer II) and *syn*-glycolamide (5.5 and 4.4 Debye, respectively).

Besides the dipole moment, the relative energies between isomers have been used traditionally to predict if a molecule might be present in the ISM. Lattelais et al. (2011) proposed that the isomers with higher abundances are those most thermodynamically stable. This empirical rule was called the Minimum Energy Principe (MEP). However, the broad variety of new isomers detected in the last years has cast serious doubts about the applicability of the MEP. It still holds for stereois-

Table 2. List of observed transitions of *syn*-glycolamide (*syn*-NH₂C(O)CH₂OH). We provide the transitions frequencies, quantum numbers, base 10 logarithm of the integrated intensity at 300 K ($\log I$), and the values of the upper levels of each transition (E_u). The last column gives the information about the species whose transitions are partially blended with *syn*-glycolamide lines.

Frequency (GHz)	Transition (J_{K_a, K_c})	$\log I$ (nm ² MHz)	E_u (K)	Blending ^a
31.9403720	5 _{1,5} - 4 _{1,4}	-5.4635	4.9	unblended
32.9834199	5 _{0,5} - 4 _{0,4}	-5.4258	4.8	unblended
34.3346824	2 _{2,1} - 1 _{1,0}	-5.7880	2.3	partially blended with U
34.7930509	5 _{2,4} - 4 _{2,3}	-5.4485	6.3	partially blended with CH ₃ COCH ₃
34.9940974	5 _{1,5} - 4 _{0,4}	-5.3948	4.9	partially blended with ¹³ CH ₃ CH ₂ CN
35.4025207	5 _{3,3} - 4 _{3,2}	-5.5525	8.0	partially blended with U
35.5265875	2 _{2,0} - 1 _{1,1}	-5.7941	1.4	blended with U
36.8706638	6 _{0,6} - 5 _{1,5}	-5.2658	6.7	unblended*
36.8711421	5 _{2,3} - 4 _{2,2}	-5.3969	6.5	unblended*
37.1038814	5 _{1,4} - 4 _{1,3}	-5.3359	5.7	unblended
38.1071149	6 _{1,6} - 5 _{1,5}	-5.2286	6.7	partially blended with U
38.8813371	6 _{0,6} - 5 _{0,5}	-5.2068	6.7	unblended
40.1177882	6 _{1,6} - 5 _{0,5}	-5.1784	6.7	unblended
41.5309974	6 _{2,5} - 5 _{2,4}	-5.1944	8.3	unblended
43.4830710	7 _{0,7} - 6 _{1,6}	-5.0310	8.8	partially blended with <i>anti</i> - and <i>syn</i> -CH ₂ CHCHNH
44.2047398	7 _{1,7} - 6 _{1,6}	-5.0327	8.9	partially blended with <i>agG</i> -(CH ₂ OH) ₂
44.7195221	7 _{0,7} - 6 _{0,6}	-5.0209	8.8	partially blended with <i>agG</i> -(CH ₂ OH) ₂
88.0821975	7 _{3,4} - 6 _{2,5}	-4.8243	12.5	unblended
97.6105934	5 _{5,1} - 4 _{4,0}	-4.4215	13.3	unblended*
97.6111554	5 _{5,0} - 4 _{4,1}	-4.4214	13.3	unblended*

(a) “U” refers to blendings with emission from an unknown (not identified) species; transitions with the * symbol are not blended with emission from other species, but (auto)blended with another transition of *syn*-glycolamide.

mers (or spatial isomers),³ such as the *anti* and *gauche* conformers of ethyl formate (CH₃CH₂(O)CHO; [Tercero et al. 2013](#); [Rivilla et al. 2017](#)), or the *Z* and *E* isomers of cyanomethanimine (HNCHCN). Their relative isomeric ratios follow the value expected according to the thermodynamic equilibrium, which scales with $\exp(-\Delta E/T_k)$, where ΔE is the energy difference between the conformers and T_k the kinetic temperature of the gas. [García de la Concepción et al. \(2021\)](#) recently demonstrated, using theoretical calculations, that this equilibrium is indeed possible in the conditions of the ISM thanks to tunneling effects that allow the isomerization.

However, it is well known that MEP fails to predict the relative abundances of many constitutional (or structural) isomers,⁴ e.g. the C₃H₂O or C₂H₄O₂ and isomeric families (see e.g. [Shingledecker et al. 2019](#) and [Mininni et al. 2020](#), respectively).

The analysis of the C₂H₅O₂N isomers presented in this work confirms that the MEP does not hold for this family either. We show in [Figure 2](#) the molecular abundances with respect to H₂ of the C₂H₅O₂N isomers as a function of its relative energies, listed in [Table 1](#). The most stable isomer with available spectroscopy is *syn*-methyl carbamate, followed by the both conformers of glycine, none of them detected towards G+0.693. Glycolamide is the next isomer in terms of relative energy. The red line in [Figure 2](#) indicates the expected molecular abundance of the C₂H₅O₂N isomers as a function of their relative energy, in case the thermodynamic equilibrium were governing the isomeric relative abundances. We have assumed a kinetic temperature of $T_k = 100$ K for G+0.693 ([Zeng et al. 2018](#)), and used the relative energy differences in [Table 1](#). From thermodynamics, N-methylcarbamic acid and both glycine conformers should have much higher abundances than glycolamide, and also higher than the upper limits derived for them (blue triangles in [Figure 2](#)). Therefore, the abundances of all the C₂H₅O₂N isomers cannot be explained in terms of thermodynamical equilibrium, and hence they need

³ Isomers that possess identical constitution, but differ in the three-dimensional orientations of their atoms.

⁴ Molecular species with the same number of atoms of each element, but arranged with different bonds between them.

to be described by chemical kinetics, i.e., by different formation and destruction routes for each isomer.

In the case of the most-searched isomer, glycine, its non-detection might not be surprising from an astrochemical point of view. While chemical compounds with functional groups such as $-\text{CH}_3$, $-\text{CH}_2\text{CH}_3$, $-\text{C}\equiv\text{N}$, $-\text{CH}_2\text{OH}$, $-\text{HCO}$, or $-\text{NH}_2$, are common, interstellar molecules with the carboxyl group ($-\text{COOH}$) are remarkably scarce. So far, only the simplest representatives, formic acid (HCOOH) and acetic (CH_3COOH), have been reported; and only very recently also carbonic acid (HOCOOH) has been also detected (Sanz-Novo et al. 2023).

Glycine ($\text{NH}_2\text{CH}_2\text{COOH}$) can be seen as the amine derivative of acetic acid (CH_3COOH), in which one H atom has been replaced by the amine group (NH_2). Thus, we can use other H/ NH_2 pairs already detected towards G+0.693 to infer the expected abundance of glycine: glycolaldehyde (HCOCH_2OH) and glycolamide ($\text{NH}_2\text{COCH}_2\text{OH}$), and ethanol ($\text{CH}_3\text{CH}_2\text{OH}$) and ethanolamine ($\text{NH}_2\text{CH}_2\text{CH}_2\text{OH}$). The glycolaldehyde/glycolamide ratio is ~ 15 (Rivilla et al. 2022a, and this work), while the ethanol/ethanolamine ratio is ~ 40 (Rivilla et al. 2021a; Rodríguez-Almeida et al. 2021a). If we assume these ratios for the acetic acid/glycine pair, and using the abundance of acetic acid reported by Sanz-Novo et al. (2023) of 3.1×10^{-10} , the abundance of glycine would be in the range $\sim (0.8-2) \times 10^{-11}$. These values are a factor of 3–8 below the upper limit derived in this work for the low-energy conformer I (Table 1). As discussed in more detail in Appendix A, if both glycine conformers were in thermodynamic equilibrium, the measured upper limit derived for the high-energy conformer (II) would translate into an upper limit for the low-energy conformer of $\sim 10^{-10}$, very similar to that derived using the conformer I itself. Hence, it is clear that the abundance of glycine towards G+0.693 is expected to be below 10^{-10} , and surely lower than that derived for its isomer glycolamide (see Figure 2).

Therefore, the chemistry that takes places in the ISM might be able to form glycine, but likely its low expected abundance makes very challenging to detect it with present-day radiotelescopes at reasonable integration times. The detection of glycolamide indicates that it can be efficiently formed under interstellar conditions. In next section we will discuss several chemical pathways that can form glycolamide in the ISM.

4.2. Formation of glycolamide

The chemistry of G+0.693 is thought to be dominated by large-scale shocks (Martín-Pintado et al. 2001; Martín et al. 2008) produced by a cloud-cloud colli-

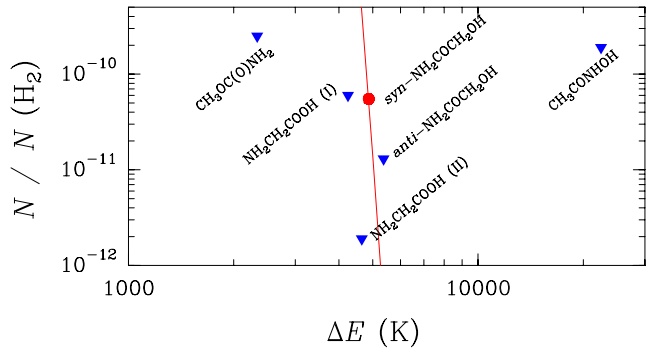


Figure 2. Molecular abundances with respect to H_2 of $\text{C}_2\text{H}_5\text{O}_2\text{N}$ isomers as a function of its relative energy (see Table 1). The red dot corresponds to the detection of *syn*-glycolamide, while the blue triangles indicate the upper limits derived for the other isomers. The solid red line indicates the expected molecular abundance of the $\text{C}_2\text{H}_5\text{O}_2\text{N}$ isomeric family assuming the thermodynamic population at $T_k = 100$ K, and using the abundance of *syn*-glycolamide as reference.

sion (Zeng et al. 2020). These shocks are responsible for the sputtering of dust grains, releasing many molecules formed on the grain surfaces into the gas phase (Caselli et al. 1997; Jiménez-Serra et al. 2008). Therefore, surface chemistry is expected to play a major role in G+0.693. For this reason, and because no viable gas-phase route of glycolamide has been proposed in the literature, from here on we will consider only grain-surface reactions.

Glycolamide is the largest molecule containing an amide functional group ($-\text{NH}-\text{C}(=\text{O})-$) detected in the ISM. It is an α -substitute of acetamide ($\text{NH}_2\text{C}(\text{O})\text{CH}_3$), in which one hydrogen atom H of the methyl group is replaced by the hydroxyl group $-\text{OH}$. Based on this similarity, both amides might have similar formation routes. The chemistry of acetamide in G+0.693 has been recently discussed by Zeng et al. (2023). Chemical models (Belloche et al. 2017, 2019; Garrod et al. 2022) have suggested that the formation of acetamide involves reactions between simple radicals (CH_3 and NH_2) with larger radicals (NH_2CO and CH_3CO) that can be synthesized on grains through H-addition and/or H-abstraction reactions of species that are abundant in the ISM, and in G+0.693 in particular (HNCO , NH_2CHO , H_2CCO , and CH_3CHO); and/or through the combination of CO with NH_2 (see the experiments of Ligterink et al. 2018) and CH_3 , respectively (see Figure 3).

Analogous pathways involving radical-radical reactions, depicted in Figure 3, are promising formation routes for glycolamide. Sanz-Novo et al. (2020) proposed that it can be formed from the reaction between NH_2 and the COCH_2OH radical. The latter can result from the H-abstraction on the formyl site of glycolaldehyde (HCOCH_2OH), the reaction between CO

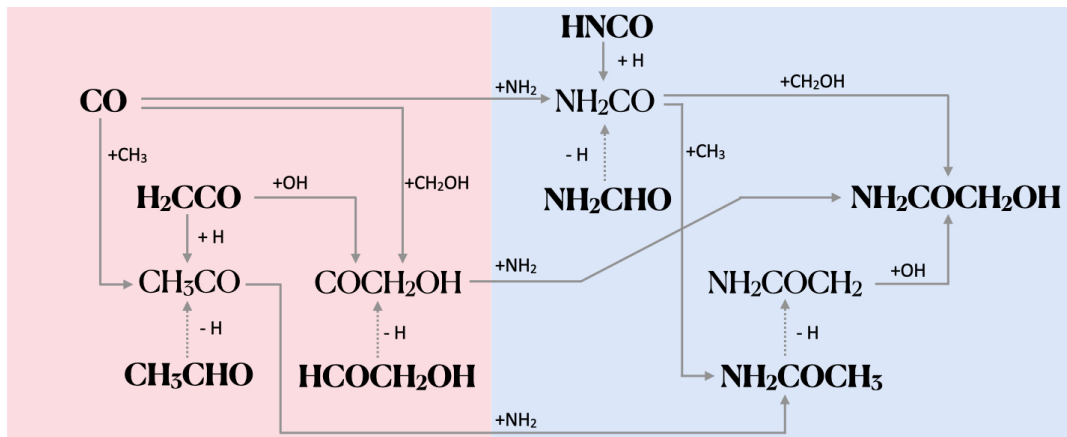


Figure 3. Proposed chemical network for the formation of glycolamide in the ISM. The left red area includes oxygen-bearing species, while the blue right panel includes nitrogen- and oxygen-bearing species. Closed-shell species are labeled in boldface, as opposed to radicals.

with the hydroxymethyl radical (CH_2OH), and/or the combination of the OH radical with ketene (H_2CCO). Haupa et al. (2020) suggested that glycolamide can also be formed through the radical-radical reaction between OH and the 2-amino-2-oxoethyl radical (NH_2COCH_2 ; Figure 3), which is formed by the H-abstraction on the methyl site of acetamide according to their experiments. A third possible route was proposed by Garrod et al. (2008): the reaction of NH_2CO (a precursor of acetamide, as mentioned above, which is formed by hydrogen abstraction from formamide), and CH_2OH (Figure 3).

All of the possible closed-shell precursors are relatively abundant towards G+0.693. Their molecular abundances with respect to H_2 , in units of 10^{-10} , are: 266 (HNCO ; Zeng et al. 2018); 37 (CH_3CHO ; Sanz-Novo et al. 2022b); 21 (H_2CCO ; Requena-Torres et al. 2008⁵); 18.5 (NH_2CHO ; Zeng et al. 2023); 8.5 (NH_2COCH_3 ; Zeng et al. 2023); and 6.9 (HCOCH_2OH ; Rivilla et al. 2022a); which are higher than the abundance of *syn*-glycolamide by factors of ~ 15 -500. Hence, all of them are viable precursors.

Besides G+0.693, abundance upper limits of glycolamide have been derived towards the hot molecular cores Sgr B2(N2), located $\sim 60''$ southwest from G+0.693, and G31.41+0.41 (hereafter G31), located in the Galactic disk (Sanz-Novo et al. 2020 and Colzi et al. 2021, respectively). We have compared in Figure 4 the column densities (normalized to acetamide,

$\text{NH}_2\text{C}(\text{O})\text{CH}_3$) derived in the three sources. We used the molecular abundances from Zeng et al. (2018), Sanz-Novo et al. (2022b), Rivilla et al. (2022a), and Zeng et al. (2023) for G+0.693; Mininni et al. (2020), Colzi et al. (2021) and private communication for G31; and Belloche et al. (2017) and Sanz-Novo et al. (2020) for Sgr B2(N2). The proposed precursors of glycolamide have similar molecular ratios in Sgr B2(N2) and G+0.693, within factors of 1.0–2.2, with the only exception of NH_2CHO , which is an order of magnitude more abundant in Sgr B2(N2) (Belloche et al. 2017). This might imply that NH_2CHO is not the dominant precursor of $\text{NH}_2\text{C}(\text{O})\text{CH}_2\text{OH}$, because in that case, the formation of glycolamide would be enhanced by the same factor toward Sgr B2(N2) as compared to the other sources.

The molecular abundance ratios in G31 are very similar to those in G+0.693 within factors ~ 1.0 –3.5, with the exceptions of CH_3CHO and $\text{NH}_2\text{C}(\text{O})\text{CH}_2\text{OH}$, which are lower by factors of ~ 10 and > 6.3 , respectively. This might indicate that acetaldehyde and glycolamide are chemically linked. However, we note that firm conclusions cannot be drawn based only on three astronomical sources, and that the detection of glycolamide in more astronomical environments (molecular clouds, hot cores/corinos, protostellar shocks) is needed to shed light on the formation processes of glycolamide.

Since radical-radical reactions on the surface of dust grains are generally barrierless, the bottleneck of the proposed pathways is the formation of the larger radicals shown in Figure 3: CH_3CO , COCH_2OH , NH_2CO , and NH_2COCH_2 . The detection of glycolamide towards G+0.693 suggests that the production of these radicals is more efficient than in Sgr B2(N2) and G31. These radicals can be formed from abundant closed-shell species by

⁵ The molecular abundance reported by Requena-Torres et al. (2008) used an H_2 column density for G+0.693 of $4.1 \times 10^{22} \text{ cm}^{-2}$, so we have recalculated it using the same value we have used for the other species, which is $1.35 \times 10^{22} \text{ cm}^{-2}$ (Martín et al. 2008).

H-abstractions, and H-, OH-, CH_3 - and NH_2 - additions (Figure 3). All these mechanisms can be enhanced in the presence of a ultraviolet field induced by cosmic rays (Garrod et al. 2022). Indeed, a high cosmic-ray ionisation rate (CRIR) has been derived towards G+0.693 ($\sim 10^{-15} - 10^{-14} \text{ s}^{-1}$, Rivilla et al. 2022b), in good agreement with those measured in its hosting Sgr B2 region (Yusef-Zadeh et al. 2007, 2016), and across the whole Galactic Center (Goto 2013). Although Sgr B2(N2) is located close to G+0.693, the extremely high column density of H_2 the hot core ($\sim 10^{26} \text{ cm}^{-2}$, Sánchez-Monge et al. 2017; much higher than that of G+0.693 of $\sim 10^{23} \text{ cm}^{-2}$) is expected to drastically attenuate the CRIR (Padovani et al. 2013). Similarly, G31 is exposed to a much lower cosmic-ray flux since it is located in the Galactic disk, where the CRIR is 2–3 orders of magnitude lower than in the Galactic Center, which is further attenuated due to the high H_2 column density of the molecular core ($\sim 10^{25} \text{ cm}^{-2}$; Mininni et al. 2020). In summary, the formation of complex molecules such as $\text{NH}_2\text{COCH}_2\text{OH}$ on the grain surfaces through filling reactions is expected to be boosted in the presence of high CRIR, like that present in G+0.693.

5. SUMMARY AND CONCLUSIONS

We have searched for members of the isomeric family of glycine ($\text{C}_2\text{H}_5\text{O}_2\text{N}$) towards the G+0.693-0.027 molecular cloud located in the Galactic Center, using new ultradeep observations carried out with the Yebes 40m and IRAM 30m telescopes with improved sensitivity at sub-mK levels. We present the first detection in the interstellar medium of a $\text{C}_2\text{H}_5\text{O}_2\text{N}$ isomer: the *syn* conformer of glycolamide ($\text{NH}_2\text{C}(\text{O})\text{CH}_2\text{OH}$). We have derived a column density of $(7.4 \pm 0.7) \times 10^{12} \text{ cm}^{-2}$, which translates into a molecular abundance with respect to molecular hydrogen of 5.5×10^{-10} . We also report upper limits of the molecular abundances of five other isomers: the *anti* conformer of glycolamide, the conformers I and II of glycine ($\text{NH}_2\text{CH}_2\text{COOH}$), *syn*-methyl carbamate ($\text{CH}_3\text{OC}(\text{O})\text{NH}_2$), and N-(Z)-hydroxyacetamide ($\text{CH}_3\text{C}(\text{O})\text{NHOH}$). The upper limit for the low-energy conformer of glycine is $< 0.6 \times 10^{-10}$, which indicates that it is less abundant than *syn*-glycolamide. The relative abundances of the $\text{C}_2\text{H}_5\text{O}_2\text{N}$ isomers cannot be described in terms of thermodynamics, and thus they are due to different chemical pathways in the ISM, which favour the formation of glycolamide over other isomers. We discuss different routes to produce glycolamide on the surface of dust grains, based on reactions between simple radicals (OH, NH_2 , CH_3 and CH_2OH) and larger radicals generated from abundant precursors already detected in the cloud (CO, HNC, CH_3CHO , NH_2CHO ,

H_2CCO , HCOCH_2OH or NH_2COCH_3) after H-, OH- and NH_2 -additions, and/or H-abstractions. The formation of these radicals is expected to be enhanced in the presence of the intense cosmic-ray secondary ultraviolet field likely present in G+0.693, providing a natural explanation for the detection of glycolamide, and opening the window for the detection of equally or even more complex species.

Software: Madrid Data Cube Analysis (MADCUBA) on ImageJ is a software developed at the Center of Astrobiology (CAB) in Madrid; <https://cab.inta-csic.es/madcuba/>; (Martín et al. 2019); GILDAS, <https://www.iram.fr/IRAMFR/GILDAS>.

ACKNOWLEDGMENTS

We acknowledge the two anonymous reviewers for their careful reading of the manuscript and their useful comments. We are grateful to the IRAM 30m and Yebes 40m telescopes staff for their help during the different observing runs. The 40m radio telescope at Yebes Observatory is operated by the Spanish Geographic Institute (IGN, Ministerio de Transportes, Movilidad y Agenda Urbana). IRAM is supported by INSU/CNRS (France), MPG (Germany) and IGN (Spain). V.M.R. acknowledges support from the project RYC2020-029387-I funded by MCIN/AEI/10.13039/501100011033. M.S.N. thanks the financial funding from the European Union - NextGenerationEU, Ministerio de Universidades and the University of Valladolid under a postdoctoral Margarita Salas Grant, as well as financial support from the Spanish Ministerio de Ciencia e Innovación (PID2020-117742GB-I00). I.J.-S., J.M.-P., L.C., A.M and A.M.-H. acknowledge funding from grants No. PID2019-105552RB-C41 and MDM-2017-0737 (Unidad de Excelencia María de Maeztu-Centro de Astrobiología, INTA-CSIC) by the Spanish Ministry of Science and Innovation/State Agency of Research MCIN/AEI/10.13039/501100011033 and by “ERDF A way of making Europe”. D.S.A acknowledges the funds provided by the Consejo Superior de Investigaciones Científicas (CSIC) and the Centro de Astrobiología (CAB) through the project 20225AT015 (Proyectos intramurales especiales del CSIC). P.dV. and B.T. thank the support from the Spanish Ministerio de Ciencia e Innovación (MICIU) through project PID2019-107115GB-C21. B.T. also thanks the Spanish MICIU for funding support from grant PID2019-106235GB-I00. J.L.A. acknowledges the fundings from Ministerio de Ciencia e Innovación (PID2019-111396GB-I00) and European Research Council ERC-2013-SyG, Grant Agreement n. 610256 NANOCOSMOS.

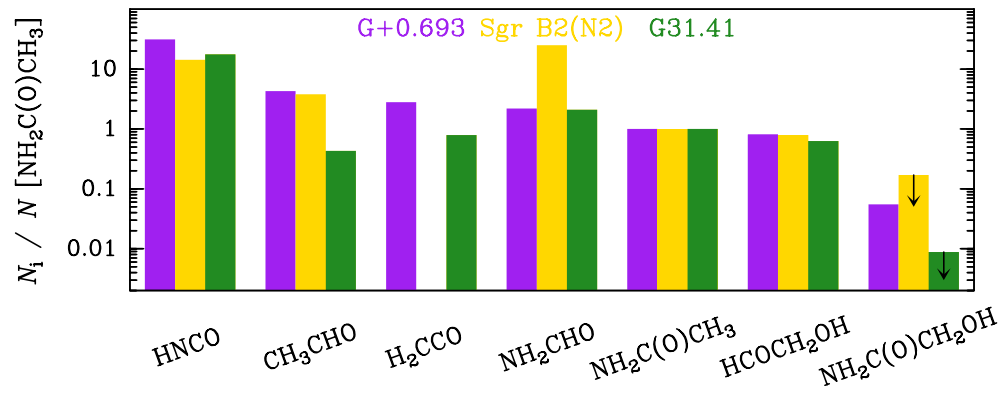


Figure 4. Comparison of the relative molecular abundances, compared to acetamide, of the proposed precursors of glycolamide, derived towards G+0.693 (purple) and the hot cores Sgr B2(N2) (yellow) and G31.41+0.31 (green). Upper limits of glycolamide are indicated with arrows.

REFERENCES

- Alberton, D., Bizzocchi, L., Jiang, N., et al. 2023, *A&A*, 669, A93, doi: [10.1051/0004-6361/202244618](https://doi.org/10.1051/0004-6361/202244618)
- Altwegg, K., Balsiger, H., Bar-Nun, A., et al. 2016, *Science Advances*, 2, e1600285, doi: [10.1126/sciadv.1600285](https://doi.org/10.1126/sciadv.1600285)
- Bakri, B., Demaison, J., Kleiner, I., et al. 2002, *Journal of Molecular Spectroscopy*, 215, 312, doi: <https://doi.org/10.1006/jmsp.2002.8647>
- Belloche, A., Garrod, R. T., Müller, H. S. P., et al. 2019, *A&A*, 628, A10, doi: [10.1051/0004-6361/201935428](https://doi.org/10.1051/0004-6361/201935428)
- Belloche, A., Meshcheryakov, A. A., Garrod, R. T., et al. 2017, *A&A*, 601, A49, doi: [10.1051/0004-6361/201629724](https://doi.org/10.1051/0004-6361/201629724)
- Bizzocchi, L., Prudenzano, D., Rivilla, V. M., et al. 2020, *A&A*, 640, A98, doi: [10.1051/0004-6361/202038083](https://doi.org/10.1051/0004-6361/202038083)
- Burton, A. S., Stern, J. C., Elsila, J. E., Glavin, D. P., & Dworkin, J. P. 2012, *Chem. Soc. Rev.*, 41, 5459, doi: [10.1039/C2CS35109A](https://doi.org/10.1039/C2CS35109A)
- Caselli, P., Hartquist, T. W., & Havnes, O. 1997, *A&A*, 322, 296
- Ceccarelli, C., Castets, A., Caux, E., et al. 2000, *Astronomy and Astrophysics*, 355, 1129, <http://adsabs.harvard.edu/abs/2000A%26A...355.1129C>
- Chyba, C., & Sagan, C. 1992, *Nature*, 355, 125, doi: [10.1038/355125a0](https://doi.org/10.1038/355125a0)
- Chyba, C. F. 1990, *Nature*, 343, 129, doi: [10.1038/343129a0](https://doi.org/10.1038/343129a0)
- Colzi, L., Rivilla, V. M., Beltrán, M. T., et al. 2021, *A&A*, 653, A129, doi: [10.1051/0004-6361/202141573](https://doi.org/10.1051/0004-6361/202141573)
- Colzi, L., Martín-Pintado, J., Rivilla, V. M., et al. 2022, *ApJL*, 926, L22, doi: [10.3847/2041-8213/ac52ac](https://doi.org/10.3847/2041-8213/ac52ac)
- Combes, F., Q-Rieu, N., & Wlodarczak, G. 1996, *A&A*, 308, 618
- Cooper, G., Kimmich, N., Belisle, W., et al. 2001, *Nature*, 414, 879, doi: [10.1038/414879a](https://doi.org/10.1038/414879a)
- Cronin, J., & Pizzarello, S. 1983, *Advances in Space Research*, 3, 5, doi: [https://doi.org/10.1016/0273-1177\(83\)90036-4](https://doi.org/10.1016/0273-1177(83)90036-4)
- Cronin, J. R., Pizzarello, S., & Cruikshank, D. P. 1988, in *Meteorites and the Early Solar System*, ed. J. F. Kerridge & M. S. Matthews, 819–857
- Csaszar, A. G. 1992, *Journal of the American Chemical Society*, 114, 9568, doi: [10.1021/ja00050a041](https://doi.org/10.1021/ja00050a041)
- Cunningham, M. R., Jones, P. A., Godfrey, P. D., et al. 2007, *MNRAS*, 376, 1201, doi: [10.1111/j.1365-2966.2007.11504.x](https://doi.org/10.1111/j.1365-2966.2007.11504.x)
- Demyk, K., Wlodarczak, G., & Dartois, E. 2004, in *SF2A-2004: Semaine de l’Astrophysique Française*, ed. F. Combes, D. Barret, T. Contini, F. Meynadier, & L. Pagani, 493
- Endres, C. P., Schlemmer, S., Schilke, P., Stutzki, J., & Müller, H. S. P. 2016, *Journal of Molecular Spectroscopy*, 327, 95, doi: [10.1016/j.jms.2016.03.005](https://doi.org/10.1016/j.jms.2016.03.005)
- García de la Concepción, J., Jiménez-Serra, I., Carlos Corchado, J., Rivilla, V. M., & Martín-Pintado, J. 2021, *ApJL*, 912, L6, doi: [10.3847/2041-8213/abf650](https://doi.org/10.3847/2041-8213/abf650)
- Garrod, R. T., Jin, M., Matis, K. A., et al. 2022, *ApJS*, 259, 1, doi: [10.3847/1538-4365/ac3131](https://doi.org/10.3847/1538-4365/ac3131)
- Garrod, R. T., Widicus Weaver, S. L., & Herbst, E. 2008, *The Astrophysical Journal*, 682, 283, doi: [10.1086/588035](https://doi.org/10.1086/588035)
- Glavin, D. P., & Dworkin, J. P. 2009, *Proceedings of the National Academy of Science*, 106, 5487, doi: [10.1073/pnas.0811618106](https://doi.org/10.1073/pnas.0811618106)
- Goto, M. 2013, *Proceedings of the International Astronomical Union*, 9, 429, doi: [10.1017/S1743921314001070](https://doi.org/10.1017/S1743921314001070)
- Groner, P., Winnewisser, M., Medvedev, I. R., et al. 2007, *ApJS*, 169, 28, doi: [10.1086/511133](https://doi.org/10.1086/511133)
- Haupa, K. A., Ong, W.-S., & Lee, Y.-P. 2020, *Physical Chemistry Chemical Physics (Incorporating Faraday Transactions)*, 22, 6192, doi: [10.1039/C9CP06279C](https://doi.org/10.1039/C9CP06279C)

- Ilyushin, V., Alekseev, E., Demaison, J., & Kleiner, I. 2006, *Journal of Molecular Spectroscopy*, 240, 127, doi: <https://doi.org/10.1016/j.jms.2006.09.008>
- Ilyushin, V., Alekseev, E., Dyubko, S., Motiyenko, R., & Lovas, F. 2005, *Journal of Molecular Spectroscopy*, 231, 15, doi: <https://doi.org/10.1016/j.jms.2004.12.003>
- Ioppolo, S., Fedoseev, G., Chuang, K. J., et al. 2021, *Nature Astronomy*, 5, 197, doi: [10.1038/s41550-020-01249-0](https://doi.org/10.1038/s41550-020-01249-0)
- Jiménez-Serra, I., Caselli, P., Martín-Pintado, J., & Hartquist, T. W. 2008, *A&A*, 482, 549, doi: [10.1051/0004-6361:20078054](https://doi.org/10.1051/0004-6361:20078054)
- Jiménez-Serra, I., Vasyunin, A. I., Caselli, P., et al. 2016, *The Astrophysical Journal Letters*, 830, L6, doi: [10.3847/2041-8205/830/1/L6](https://doi.org/10.3847/2041-8205/830/1/L6)
- Jiménez-Serra, I., Martín-Pintado, J., Rivilla, V. M., et al. 2020, *Astrobiology*, 20, 1048, doi: [10.1089/ast.2019.2125](https://doi.org/10.1089/ast.2019.2125)
- Jiménez-Serra, I., Rodríguez-Almeida, L. F., Martín-Pintado, J., et al. 2022, *A&A*, 663, A181, doi: [10.1051/0004-6361/202142699](https://doi.org/10.1051/0004-6361/202142699)
- Jones, P. A., Cunningham, M. R., Godfrey, P. D., & Cragg, D. M. 2007, *MNRAS*, 374, 579, doi: [10.1111/j.1365-2966.2006.11175.x](https://doi.org/10.1111/j.1365-2966.2006.11175.x)
- Kuan, Y.-J., Charnley, S. B., Huang, H.-C., Tseng, W.-L., & Kisiel, Z. 2003, *ApJ*, 593, 848, doi: [10.1086/375637](https://doi.org/10.1086/375637)
- Lattalais, M., Pauzat, F., Pilmé, J., Ellinger, Y., & Ceccarelli, C. 2011, *A&A*, 532, A39, doi: [10.1051/0004-6361/201016039](https://doi.org/10.1051/0004-6361/201016039)
- Ligterink, N. F. W., Calcutt, H., Coutens, A., et al. 2018, *A&A*, 619, A28, doi: [10.1051/0004-6361/201731980](https://doi.org/10.1051/0004-6361/201731980)
- Lovas, F. J., Kawashima, Y., Grabow, J. U., et al. 1995, *ApJL*, 455, L201, doi: [10.1086/309844](https://doi.org/10.1086/309844)
- Maris, A. 2004, *Physical Chemistry Chemical Physics*, 6, 2611
- Marstokk, K., & Mollandal, H. 1999, *Acta Chemica Scandinavica*, 53, 79
- Martín, S., Martín-Pintado, J., Blanco-Sánchez, C., et al. 2019, *A&A*, 631, A159, doi: [10.1051/0004-6361/201936144](https://doi.org/10.1051/0004-6361/201936144)
- Martín, S., Requena-Torres, M. A., Martín-Pintado, J., & Mauersberger, R. 2008, *The Astrophysical Journal*, 678, 245, doi: [10.1086/533409](https://doi.org/10.1086/533409)
- Martín-Pintado, J., Rizzo, J. R., de Vicente, P., Rodríguez-Fernández, N. J., & Fuente, A. 2001, *ApJL*, 548, L65, doi: [10.1086/318937](https://doi.org/10.1086/318937)
- Marty, B., Altwegg, K., Balsiger, H., et al. 2017, *Science*, 356, 1069, doi: [10.1126/science.aal3496](https://doi.org/10.1126/science.aal3496)
- Megías, A., Jiménez-Serra, I., Martín-Pintado, J., et al. 2023, *MNRAS*, 519, 1601, doi: [10.1093/mnras/stac3449](https://doi.org/10.1093/mnras/stac3449)
- Mininni, C., Beltrán, M. T., Rivilla, V. M., et al. 2020, *A&A*, 644, A84, doi: [10.1051/0004-6361/202038966](https://doi.org/10.1051/0004-6361/202038966)
- Muñoz Caro, G. M., Meierhenrich, U. J., Schutte, W. A., et al. 2002, *Nature*, 416, 403, doi: [10.1038/416403a](https://doi.org/10.1038/416403a)
- O'Brien, D. P., Izidoro, A., Jacobson, S. A., Raymond, S. N., & Rubie, D. C. 2018, *SSRv*, 214, 47, doi: [10.1007/s11214-018-0475-8](https://doi.org/10.1007/s11214-018-0475-8)
- Oró, J. 1961, *Nature*, 190, 389, doi: [10.1038/190389a0](https://doi.org/10.1038/190389a0)
- Padovani, M., Hennebelle, P., & Galli, D. 2013, *A&A*, 560, A114, doi: [10.1051/0004-6361/201322407](https://doi.org/10.1051/0004-6361/201322407)
- Pasek, M. A. 2008, *Proceedings of the National Academy of Sciences*, 105, 853
- Pearce, B. K., Pudritz, R. E., Semenov, D. A., & Henning, T. K. 2017, *Proceedings of the National Academy of Sciences*, 114, 11327, doi: [10.1073/pnas.1710339114](https://doi.org/10.1073/pnas.1710339114)
- Pickett, H. M., Poynter, R. L., Cohen, E. A., et al. 1998, *JQSRT*, 60, 883, doi: [10.1016/S0022-4073\(98\)00091-0](https://doi.org/10.1016/S0022-4073(98)00091-0)
- Pizzarello, S., Cooper, G. W., & Flynn, G. J. 2006, *The Nature and Distribution of the Organic Material in Carbonaceous Chondrites and Interplanetary Dust Particles*, ed. D. S. Lauretta & H. Y. McSween, 625
- Potiszil, C., Ota, T., Yamanaka, M., et al. 2023, *Nature Communications*, 14, 1482, doi: [10.1038/s41467-023-37107-6](https://doi.org/10.1038/s41467-023-37107-6)
- Requena-Torres, M. A., Martín-Pintado, J., Martín, S., & Morris, M. R. 2008, *The Astrophysical Journal*, 672, 352, doi: [10.1086/523627](https://doi.org/10.1086/523627)
- Requena-Torres, M. A., Martín-Pintado, J., Rodríguez-Franco, A., et al. 2006, *Astronomy & Astrophysics*, 455, 971, doi: [10.1051/0004-6361:20065190](https://doi.org/10.1051/0004-6361:20065190)
- Rivilla, V. M., Beltrán, M. T., Martín-Pintado, J., et al. 2017, *Astronomy and Astrophysics*, 599, A26, doi: [10.1051/0004-6361/201628823](https://doi.org/10.1051/0004-6361/201628823)
- Rivilla, V. M., Jiménez-Serra, I., Zeng, S., et al. 2018, *MNRAS*, 475, L30, doi: [10.1093/mnrasl/slx208](https://doi.org/10.1093/mnrasl/slx208)
- Rivilla, V. M., Martín-Pintado, J., Jiménez-Serra, I., et al. 2019, *MNRAS*, 483, L114, doi: [10.1093/mnrasl/sly228](https://doi.org/10.1093/mnrasl/sly228)
- Rivilla, V. M., Drozdovskaya, M. N., Altwegg, K., et al. 2020a, *MNRAS*, 492, 1180, doi: [10.1093/mnras/stz3336](https://doi.org/10.1093/mnras/stz3336)
- Rivilla, V. M., Martín-Pintado, J., Jiménez-Serra, I., et al. 2020b, *ApJL*, 899, L28, doi: [10.3847/2041-8213/abac55](https://doi.org/10.3847/2041-8213/abac55)
- Rivilla, V. M., Jiménez-Serra, I., Martín-Pintado, J., et al. 2021a, *Proceedings of the National Academy of Science*, 118, 2101314118, doi: [10.1073/pnas.2101314118](https://doi.org/10.1073/pnas.2101314118)
- Rivilla, V. M., Jiménez-Serra, I., García de la Concepción, J., et al. 2021b, *MNRAS*, 506, L79, doi: [10.1093/mnrasl/slab074](https://doi.org/10.1093/mnrasl/slab074)
- Rivilla, V. M., Colzi, L., Jiménez-Serra, I., et al. 2022a, *ApJL*, 929, L11, doi: [10.3847/2041-8213/ac6186](https://doi.org/10.3847/2041-8213/ac6186)
- Rivilla, V. M., García De La Concepción, J., Jiménez-Serra, I., et al. 2022b, *Frontiers in Astronomy and Space Sciences*, 9, 829288, doi: [10.3389/fspas.2022.829288](https://doi.org/10.3389/fspas.2022.829288)

- Rivilla, V. M., Jiménez-Serra, I., Martín-Pintado, J., et al. 2022c, *Frontiers in Astronomy and Space Sciences*, 9, 876870, doi: [10.3389/fspas.2022.876870](https://doi.org/10.3389/fspas.2022.876870)
- Rodríguez-Almeida, L. F., Jiménez-Serra, I., Rivilla, V. M., et al. 2021a, *ApJL*, 912, L11, doi: [10.3847/2041-8213/abf7cb](https://doi.org/10.3847/2041-8213/abf7cb)
- Rodríguez-Almeida, L. F., Rivilla, V. M., Jiménez-Serra, I., et al. 2021b, *A&A*, 654, L1, doi: [10.1051/0004-6361/202141989](https://doi.org/10.1051/0004-6361/202141989)
- Rubin, M., Bekaert, D. V., Broadley, M. W., Drozdovskaya, M. N., & Wampfler, S. F. 2019, *ACS Earth and Space Chemistry*, 3, 1792, doi: [10.1021/acsearthspacechem.9b00096](https://doi.org/10.1021/acsearthspacechem.9b00096)
- San Andrés, D., Colzi, L., Rivilla, V. M., et al. 2023, *MNRAS*, doi: [10.1093/mnras/stad1385](https://doi.org/10.1093/mnras/stad1385)
- Sánchez-Monge, Á., Schilke, P., Schmiedeke, A., et al. 2017, *A&A*, 604, A6, doi: [10.1051/0004-6361/201730426](https://doi.org/10.1051/0004-6361/201730426)
- Sanz-Novo, M., Alonso, J. L., Rivilla, V. M., et al. 2022a, *A&A*, 666, A134, doi: [10.1051/0004-6361/202244330](https://doi.org/10.1051/0004-6361/202244330)
- Sanz-Novo, M., Largo, A., Redondo, P., & Barrientos, C. 2019, *ACS Earth and Space Chemistry*, 3, 1170, doi: [10.1021/acsearthspacechem.9b00053](https://doi.org/10.1021/acsearthspacechem.9b00053)
- Sanz-Novo, M., Belloche, A., Alonso, J. L., et al. 2020, *A&A*, 639, A135, doi: [10.1051/0004-6361/202038149](https://doi.org/10.1051/0004-6361/202038149)
- Sanz-Novo, M., Belloche, A., Rivilla, V. M., et al. 2022b, *A&A*, 666, A114, doi: [10.1051/0004-6361/202142848](https://doi.org/10.1051/0004-6361/202142848)
- Sanz-Novo, M., Rivilla, V. M., Jiménez-Serra, I., et al. 2023, *arXiv e-prints*, arXiv:2307.08644, doi: [10.48550/arXiv.2307.08644](https://doi.org/10.48550/arXiv.2307.08644)
- Shingledecker, C. N., Álvarez-Barcia, S., Korn, V. H., & Kästner, J. 2019, *ApJ*, 878, 80, doi: [10.3847/1538-4357/ab1d4a](https://doi.org/10.3847/1538-4357/ab1d4a)
- Snyder, L. E., Lovas, F. J., Hollis, J. M., et al. 2005, *ApJ*, 619, 914, doi: [10.1086/426677](https://doi.org/10.1086/426677)
- Tercero, B., Kleiner, I., Cernicharo, J., et al. 2013, *The Astrophysical Journal Letters*, 770, L13, doi: [10.1088/2041-8205/770/1/L13](https://doi.org/10.1088/2041-8205/770/1/L13)
- Tercero, F., López-Pérez, J. A., Gallego, J. D., et al. 2021, *A&A*, 645, A37, doi: [10.1051/0004-6361/202038701](https://doi.org/10.1051/0004-6361/202038701)
- Yusef-Zadeh, F., Cotton, W., Wardle, M., & Intema, H. 2016, *ApJL*, 819, L35, doi: [10.3847/2041-8205/819/2/L35](https://doi.org/10.3847/2041-8205/819/2/L35)
- Yusef-Zadeh, F., Muno, M., Wardle, M., & Lis, D. C. 2007, *ApJ*, 656, 847, doi: [10.1086/510663](https://doi.org/10.1086/510663)
- Zeng, S., Jiménez-Serra, I., Rivilla, V. M., et al. 2018, *Monthly Notices of the Royal Astronomical Society*, 478, 2962, doi: [10.1093/mnras/sty1174](https://doi.org/10.1093/mnras/sty1174)
- Zeng, S., Zhang, Q., Jiménez-Serra, I., et al. 2020, *MNRAS*, 497, 4896, doi: [10.1093/mnras/staa2187](https://doi.org/10.1093/mnras/staa2187)
- Zeng, S., Jiménez-Serra, I., Rivilla, V. M., et al. 2021, *ApJL*, 920, L27, doi: [10.3847/2041-8213/ac2c7e](https://doi.org/10.3847/2041-8213/ac2c7e)
- Zeng, S., Rivilla, V. M., Jiménez-Serra, I., et al. 2023, *MNRAS*, doi: [10.1093/mnras/stad1478](https://doi.org/10.1093/mnras/stad1478)

APPENDIX

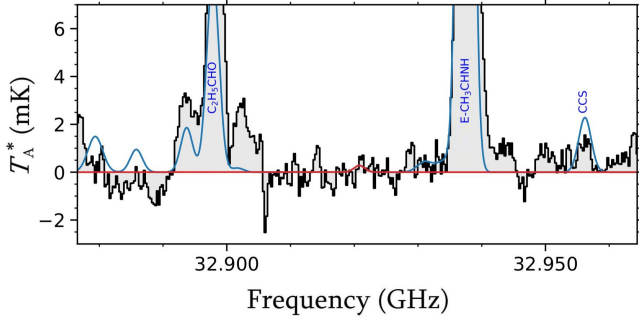


Figure A1. Transition of *anti*-glycolamide (*anti*- $\text{NH}_2\text{C}(\text{O})\text{CH}_2\text{OH}$) used to derive its column density upper limit. The observed spectra are shown as a grey histogram, and the LTE synthetic model using the derived upper limit is shown with a red curve.

A. UPPER LIMITS OF NON-DETECTED $\text{C}_2\text{H}_5\text{O}_2\text{N}$ ISOMERS

We have also searched for other $\text{C}_2\text{H}_5\text{O}_2\text{N}$ isomers for which rotational spectroscopy is available, which are not detected. We have thus derived 3σ upper limits for their molecular abundances, where σ is the root mean square noise of the spectra. We used the brightest transitions predicted by the LTE model that appear completely unblended, which are listed in Table A1. For consistency, we used the same T_{ex} , v_{LSR} , and FWHM values of the detected *syn* conformer of glycolamide.

For the high-energy *anti* conformer of glycolamide, we imported into SLIM the spectroscopic parameters reported in Table 2 of Sanz-Novo et al. (2020), which include the experimental measurements and dipole moment calculations from Maris (2004). We used the hyperfine transitions $5_{0,5}-4_{0,4}$ (at 32.9205744 and 32.9208273 GHz), shown in Figure A1. We obtained $N < 1.7 \times 10^{12} \text{ cm}^{-2}$, which translates into a molecular abundance compared to H_2 of 0.13×10^{-10} (Table 1). The derived *syn/anti* ratio is > 4.4 , which is consistent with the one predicted if both conformers follow thermodynamic equilibrium, as observed for other species in the ISM (e.g. Rivilla et al. 2017; Rivilla et al. 2019; García de la Concepción et al. 2021). Using their relative energy difference ($\Delta E = 501$ K, see Table 1), and using a kinetic temperature of $T_{\text{k}} = 100$ K for G+0.693 (Zeng et al. 2018), their expected relative ratio would be *syn/anti* > 150 , which indicates that the detection of the *anti* conformer would be challenging.

For the conformers I and II of glycine ($\text{NH}_2\text{CH}_2\text{COOH}$) we used the Cologne Database for

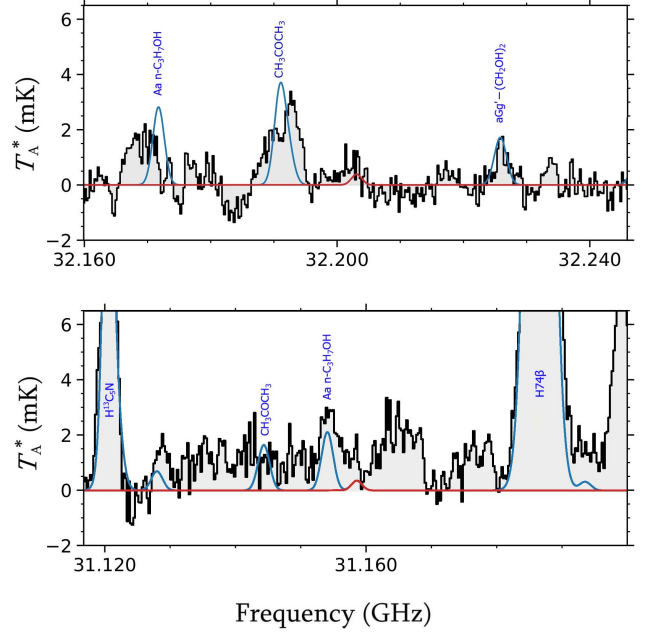


Figure A2. Transitions of the conformer I of glycine ($\text{NH}_2\text{CH}_2\text{COOH}$) used to derive its column density upper limit. The observed spectra are shown as a grey histogram, and the LTE synthetic model using the derived upper limit is shown with a red curve.

Molecular Spectroscopy (CDMS, Endres et al. 2016) entries 75511 and 75512, respectively. For conformer I, we used the transitions $5_{1,5}-4_{1,4}$ and $5_{0,4}-4_{0,4}$ at 31.1583057 and 32.2028617 GHz, respectively. For conformer II, we used the transition $6_{2,5}-5_{2,4}$ at 41.9020415 GHz, respectively. These transitions are shown in Figure A2 and A3, respectively. We obtained $N < 8.1 \times 10^{12} \text{ cm}^{-2}$ and $N < 2.5 \times 10^{11} \text{ cm}^{-2}$ for glycine conformers I and II, respectively. The upper limits of molecular abundances are $< 0.6 \times 10^{-10}$ and $< 0.019 \times 10^{-10}$, respectively (Table 1). The upper limit derived for the high-energy conformer II is much lower because its dipole moment is larger by a factor of 5 (see Table 1). If both conformers were in thermodynamic equilibrium, from the upper limit of the conformer II we could predict the expected column density of conformer I. Using their relative energy ($\Delta E = 403$ K, see Table 1), and assuming $T_{\text{k}} = 100$ K, the ratio between the conformers would be ~ 56 . Using this ratio, the upper limit of the low-energy conformer I would be $\sim 1 \times 10^{-10}$, very similar to that derived directly using conformer I transitions (Table 1).

Table A1. Transitions used to compute the molecular abundance upper limits for the $C_2H_5O_2N$ isomers not detected towards G+0.693. We provide the quantum numbers, transitions frequencies, base 10 logarithm of the integrated intensity at 300 K ($\log I$), and the values of the upper levels for each transitions (E_u).

Species	Formula	Transition	Frequency (GHz)	$\log I$ (nm^2 MHz)	E_u (K)
<i>anti</i> -glycolamide	$NH_2C(O)CH_2OH$	$5_{0,5,6} - 4_{0,4,5}^{(a)}$	32.9205744	-5.9032	4.8
		$5_{0,5,5} - 4_{0,4,4}$	32.9208273	-5.9935	4.8
glycine (conformer I)	NH_2CH_2COOH	$5_{1,5} - 4_{1,4}^{(b)}$	31.1583057	-6.5064	4.8
		$5_{0,4} - 4_{0,4}$	32.2028617	-6.4669	4.7
glycine (conformer II)	NH_2CH_2COOH	$6_{2,5} - 5_{2,4}^{(b)}$	41.9020415	-4.6541	8.3
<i>syn</i> -methyl carbamate	$CH_3OC(O)NH_2$	$2_{2,0,2} - 1_{1,1,1} A^{(c,d)}$	36.7150325	-7.1378	2.4
		$2_{2,0,2} - 1_{1,1,2} A$	36.7156362	-7.6149	2.4
		$2_{2,0,1} - 1_{1,1,1} A$	36.7164348	-7.6150	2.4
		$2_{2,0,3} - 1_{1,1,2} A$	36.7165377	-6.8668	2.4
		$2_{2,0,1} - 1_{1,1,0} A$	36.7179444	-7.4900	2.4
N-(Z)-hydroxyacetamide	$CH_3C(O)NHOH$	$6_{1,6,7} - 5_{0,5,6} A^{(d)}$	40.8305064	-6.6448	6.9

NOTE—^(a) For *anti*-glycolamide and N-(Z)-hydroxyacetamide the Hamiltonian was set up in the coupled basis set $I + J = F$, so the energy levels involved in each transition are labeled with the quantum numbers J , K_a , K_c , and F . ^(b) For the glycine conformers, the quantum numbers are J , K_a and K_c . ^(c) For *syn*-methyl carbamate, an internal rotor Hamiltonian was used and the hyperfine structure was also considered. ^(d) The A label refers to the A -symmetry state of *syn*-methyl carbamate and N-(Z)-hydroxyacetamide, respectively, which is due in both cases to the presence of a methyl internal rotation motion.

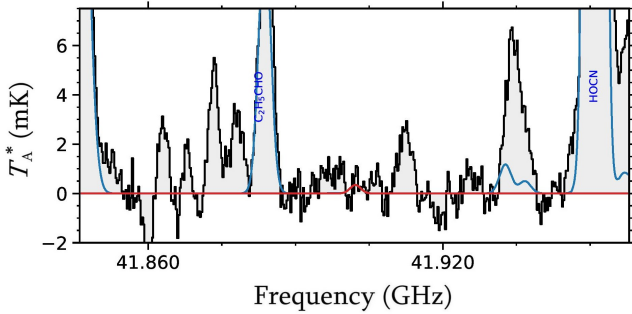


Figure A3. Transitions of the conformer II of glycine (NH_2CH_2COOH) used to derive its column density upper limit. The observed spectra are shown as a grey histogram, and the LTE synthetic model using the derived upper limit is shown with a red curve.

Syn-Methyl carbamate ($CH_3OC(O)NH$) is the lowest-energy $C_2H_5O_2N$ isomer for which rotational spectroscopy is available (Table 1). To compute its abundance upper limit, we used the Jet Propulsion Laboratory catalog (JPL; Pickett et al. 1998) entry 75004. We used the five hyperfine components of the $2_{2,0} - 1_{1,1}$ transition at ~ 36.72 GHz (Figure A4), which provides $N < 3.3 \times 10^{13} cm^{-2}$, i.e. a molecular abundance of $< 2.5 \times 10^{-10}$ (Table 1).

Similar to glycolamide, N-hydroxyacetamide (or acetohydroxamic acid, $CH_3CONHOH$) is a derivative of acetamide, in which an H atom of the amine group is replaced by the hydroxyl group. Its lower-energy con-

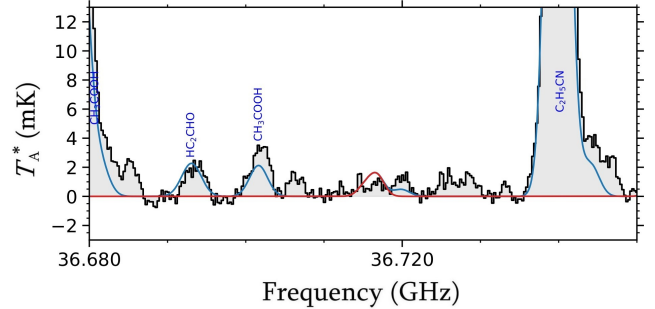


Figure A4. Transition of *syn*-methyl carbamate ($CH_3OC(O)NH_2$) used to derive its column density upper limit. The observed spectra are shown as a grey histogram, and the LTE synthetic model using the derived upper limit is shown with a red curve.

former is the Z-conformer, whose spectroscopy was presented in Sanz-Novo et al. (2022a). Although an upper limit towards G+0.693 was also reported in this work, we recalculate it here using the new deeper observations, and using the same values of T_{ex} , v_{LSR} , and FWHM values used for the other $C_2H_5O_2N$ isomers. To derive the upper limit to the column density, we have used the $6_{1,6} - 5_{0,5}$ transition at 40.8305064 GHz (Figure A5), which was also used by Sanz-Novo et al. (2022a). We obtained $N < 2.3 \times 10^{13} cm^{-2}$, i.e. a molecular abundance of $< 1.7 \times 10^{-10}$ (Table 1), slightly lower than that reported by Sanz-Novo et al. (2022a) using previous observations and assuming $T_{ex} = 8$ K, and FWHM = 20 $km s^{-1}$.

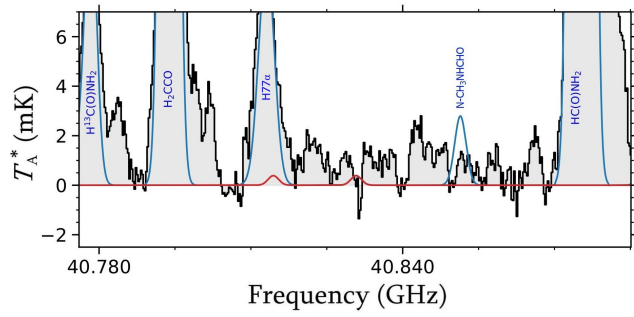


Figure A5. Transition of N-(Z)-hydroxyacetamide ($\text{CH}_3\text{C}(\text{O})\text{NHOH}$) used to derive its column density upper limit. The observed spectra are shown as a grey histogram, and the LTE synthetic model using the derived upper limit is shown with a red curve.